The composition of edible oils modifies β-sitosterol/γ-oryzanol oleogels part I: purified triglyceride oils

Authors:
Maria Scharfe, Daniel Prange, Eckhard Flöter
Department of Food Processing, Technical University Berlin, Berlin, Germany

Running Title:

Corresponding author:
Maria Scharfe,
Seestrasse 13, 13353 Berlin, Germany
+493031427588
maria.scharfe@tu-berlin.de

Abstract
The role of solvent composition, in particular, minor oil components on sterol/sterol ester oleogels, has been studied recently [1]. Reportedly, deterioration products hamper network formation and modify the gel's macroscopic properties, probably due to alterations of the scaffolding elements' interactions. However, the role of the FA composition of TAGs has not yet been addressed. In this study, minor oil components of three vegetable oils with varying degrees of unsaturation (iodine values) were removed, and the oils were chemically and physically characterized before and after the treatment. Consequently, β-sitostero/γ-oryzanol oleogels were produced, and the gel-sol (DSC) and sol-gel (rheology) transitions were monitored. Moreover, large and small deformation tests were performed, and the results were linked to oil parameters. In contrast to minor oil components, the FA composition has little impact on oleogel properties. The decline in gel hardness with IV is possibly linked to a lower solvent viscosity. However, a considerable drop in gel-sol transition temperature was observed with increasing IV indicating fewer elements of scaffolding. That was linked to the rapid formation of primary oxidation products in purified flaxseed oil during oleogel preparation, impairing tube formation. Similar to previous results on deterioration products, these minor components seem to aid network strength at low concentrations resulting in similar transition enthalpies and G'. That might be due to shifted network interactions in the presence of molecular species with functional groups. In the second part of this study, these modified interactions in the presence of selected minor components will be discussed.

1. Introduction

Besides waxes and ethylcellulose, the combination of γ-oryzanol and phytosterols is among the most promising candidates to replace traditional crystalline triglycerides (TAGs) for the structuring of semi-solid lipid phases in numerous products. In contrast to networks obtained by high levels of saturated fatty acids (SAFAs), several positive effects on human health are associated with the consumption of plant phytosterols, such as reduced blood cholesterol levels since they interfere with cholesterol absorption in the intestine [2–6]. The network is generated in a two-step gelation process. Initially, γ-oryzanol self-assembles with phytosterols into nanoscale hollow tubes. Subsequently, the individual tubules connect and form bundles, resulting in a space-filling 3D-network and a firm, translucent gel. The tube's core diameter is approximately 7.9 ±1.12 nm diameter plus the shell formed by the ferulic acid moiety of γ-oryzanol (0.8 ±0.65 nm), protruding into the surrounding liquid and forming the outer shell [7]. The moiety can form non-covalent interactions within the helix, enhancing its stability (intra-tube) [8]. The same interactions - in particular van der Waals interactions and π-π contacts - occur when

individual fibrils stick together. These are responsible for tube-tube (inter-tube) interactions and the solidification of the lipid phase [8]. Therefore, a shift from intra- to inter-tube interactions can be assumed when individual fibrils stick together. Nevertheless, interaction points are not static, but their number relates to the quantity of material (n), assuming that all molecules participate in tube formation.
However, other molecules likely develop similar interactions with the ferulic acid moiety resulting in modified inter-tube interactions and spatial arrangement of the network [1, 9]. Whether and to what extent these changes relate to the FAs composition of TAG oils has not been studied yet. Unfortunately, studies addressing this issue often comprise edible oils without further characterization or solvents with very diverse chemical structures, introducing other variables such as viscosity differences.
In a first attempt, the dependency of solvent type (decane, limonene, eugenol, sunflower oil, and castor oil) and oleogel properties such as gel formation was assessed [10]. The authors found that the molecular self-assembly is enthalpy driven and fostered in low-polar solvents, meaning that tubes form at higher temperatures and lower structurants concentration. There was no clear correlation between aggregation temperature, critical aggregation concentration, and increasing values of the dielectric constant. That might relate to the development of structures other than the nanoscale hollow tubules formed by sterols and sterol esters since the study comprised chemically mixed solvents with a wide range of permittivities (ε between 2.0-10.4), likely modifying the solubility of structurants, among other things. Reportedly, gels prepared with less polar solvents (decane, limonene) appeared opaque.
Indeed, oryzanol solubility is substantially increased in highly polar solvents [11]. A sevenfold increase of solvent permittivity (1.8 to 13.3) resulted in 7.4 times more oryzanol dissolved (hexane vs. hexanol). The increase in solubility is likely related to stronger interactions of ferulic acid moiety with the respective solvent. Although the data does not allow drawing meaningful conclusions about oryzanol solubility in edible oils, slight changes within the permittivity range of edible oils (ε~2.9-3.2) are likely. Hence, minor modifications of oryzanol solubility can be expected depending on the oils' permittivity (in purified oils) and minor polar components, resulting in fewer tubes in oils with a higher permittivity.
However, the data presented by Sawalha et al. indicates that the solvent type profoundly affects sterol-ester/sterol oleogel properties and formation [10]. Still, it seems that convincing correlations are not achievable when chemically diverse solvents are used that modify the structurants' solubility and tube formation. Hence, data linkage and comparability are limited.
In another study, the effects of oil type (flaxseed, sunflower, and extra virgin olive oil, triolein and castor oil) and oil viscosity on β-sitosterol and γ-oryzanol oleogels (gel-sol transition, firmness) were evaluated [12]. The authors argued increasing solvent viscosity negatively correlates to gel hardness due to reduced molecular mobility of β-sitosterol and γ-oryzanol. In viscous solvents, diffusion is slowed, and the chance of coinciding during the self-assembly is impeded. Interestingly, extra virgin olive and flaxseed oil oleogels showed similar hardness, although their viscosity diverges. That indicates that other factors are influencing oleogel hardness. The gel-sol transition temperatures decreased with oil polarity and viscosity. Thus, the amount of the scaffolding elements (tubules) is lower in polar oils. That might result from a combination of high viscosity in, e.g., castor oil (19 times higher, ε~4.5) and increased solubility caused by interactions of oryzanol with ricinoleic acid.
Unfortunately, these studies exclusively utilized commercially available oils without further characterization. A detailed characterization or standardization of oils is inevitable since already small changes in the composition and concentration of secondary oil components such as free fatty acids could strongly impact oleogel properties [1]. The study aimed to disentangle the role of solvent composition on β-sitosterol/γ-oryzanol oleogels with emphasis on deterioration products formed during thermal degradation at 180°C [1]. Moreover, minor oil components were almost completely removed from refined oils. Subsequently, the impact of oil composition on oleogel formation, microstructure, and macroscopic properties such as firmness was determined. The authors reported a maximum in gel firmness for briefly heated oils. Purified and more deteriorated oils were less stiff, which was associated with a modified network appearance. Indeed, atomic force microscopy revealed that the alignment and thickness of tubule bundles were altered by removing or increasing minor components' levels. This suggests that modified network interactions result in a different arrangement of scaffolding elements. However, interpretations partly suffered from inconsistency since the intense thermal treatment resulted

in numerous types of polar molecules and a partial teardown of TAGs containing PUFAs. Moreover, differences in purified triglyceride oils were observed.
Reliable implementations of oleogels are thus hard to achieve if there is only a superficial understanding of the role of oil composition. To further elucidate these effects on oleogel properties, it is necessary to consider the contribution of minor components and the bulk solvent (fatty acid profile of TAGs) separately. Moreover, the superimposition of other factors (e.g., viscosity) contributing to the changes in sterol/sterol ester oleogels should be kept to a minimum. Purification and characterization of oils reduce undesired factors contributing to oleogel network changes. That is necessary to allow for reliable data comparison and comprehensice interpretation.
Hence, the first part of this study aims to gain more insight into sterol/sterol ester oleogels formed in purified triglyceride oils with varying iodine values (IV). To this end, three edible oils (canola, sunflower, and flaxseed) with different degrees of unsaturation were purified via column chromatography and utilized in sterol/sterol ester oleogels. In contrast, the second part focuses on the changes caused by selected types of polar minor oil components.

2. Material and methods

2.1 Material

For all experiments a phytosterol mix (78.5% β-sitosterol, 10.3% sitostanol, 8.7% campesterol, 0.9% campestanol, Acros, [83-46-5],) and γ-oryzanol (purity > 98%, IMCD 26 Benelux B.V., [11042-64-1]) were used. One should note that sitostanol, campesterol, and campestanol are chemically very similar to β-sitosterol and consequently show similar gelling behavior [13]. Canola oil (Canolin 10770,) and sunflower oil (Sonnin 70020) were kindly provided by Walter Rau AG, Neuss, Germany. A 5 l container of flaxseed oil was purchased from Lausitzer Ölmühle Hoyerswerda GmbH (Hoyerswerda, Germany) and used for all experiments. All oils were stored in opaque containers at 3 °C immediately after delivery to prevent deterioration reactions.

2.2 Oil purification

Untreated canola, sunflower, and flaxseed oil were purified by combining the official method for the determination of polar compounds and two methods developed in previous studies [DGF C-III 3b (13)] [14, 15]. Briefly, the oils were mixed with an equal volume of hexane (technical grade, VWR International, Pennsylvania, USA) and subsequently passed a chromatographic column (diameter 20 mm, length 450 mm) packed with a 60 g mixture of activated aluminum oxide (activity grade: Super I, MP Biomedicals) and silica gel (60–200 µm mesh, VWR International) suspended in hexane. The flow through the column was set to 0.4–0.5 ml min^{-1}. The column and the flasks collecting the solution were wrapped in aluminum foil to prevent light-induced oxidation processes. Subsequently, the solvent was removed in a rotary evaporator at 45 °C under vacuum conditions. Traces of hexane were flushed with nitrogen, and the samples were stored at -25 °C before analysis.

2.3 Oil analysis

Water content, peroxide value, and free fatty acids. The water content, free fatty acids (FFA), and peroxide value (PV) of oil samples were determined by titration (Excellence T5, Mettler Toledo, Columbus, USA). The PV was determined according to DGF method C-VI 6a Part 2(02) (Wheeler method). Briefly, 3–5 g oil was diluted in a mixture of chloroform and acetic acid (3:2 v/v, AppliChem GmbH, Darmstadt, Germany). Subsequently, 1 ml of saturated potassium iodate (GPR RECTAPUR, VWR International, Pennsylvania, USA) solution was added. After 180 s at 30 % maximum stirring speed (~300 rpm), 50 ml of deionized water were added. The titration was performed with 10.0 mol $^{-1}$ sodium thiosulfate (Alfa Aesar, Haverhill, USA) and a redox electrode (DMi140-SC, Mettler Toledo, Columbus, USA).
The water content was determined according to DGF C-III 13a (97) (volumetric Karl Fischer method) with a voltammetric electrode (DM143-SC, Mettler Toledo, Columbus, USA). The CombiSolvent Oil Aquastar was used to dissolve about 10 g oil. The titration was carried out using the Combi Solvent Oil and the CombiTitrant 2 Aquastar 1 ml/2 mg H_2O with one-component reagents (both from Merck Millipore,

Billerica, USA). The titer was determined at least three times each day using a 1% water-standard (1 g/10 mg H_2O) (Apura, Merck Millipore, Billerica, USA).
The content of free fatty acids, expressed as oleic acid content in mg/100 g, was determined according to DGF method C-III 4 (06) with a pH electrode (DG113-SC, Mettler Toledo, Columbus, USA). Briefly, 2-4 g of oil was dissolved in 60 ml of an ethanol/diethyl ether solution (1:1 v/v, both HPLC-grade, VWR International, Pennsylvania, USA). The titration was performed using potassium hydroxide (GPR RECTAPUR, VWR International Pennsylvania, USA) in ethanol (0.02 mol/l). A blank value was determined for each new batch of solvent. The titer was determined by dissolving 25 mg benzoic acid (GPR RECTAPUR, VWR International Pennsylvania, USA) in the solvent and was measured in triplicates every day.
All measurements using titration were carried out in triplicates.

Density and refractive index. The density and refractive index were determined using a Samplify P autosampler connected to an oscillating U-tube device (EDM 5000) and a precision refractometer (ATR-C) provided by Schmidt + Haensch GmbH & Co. (Berlin, Germany). Measurements were carried out at 40 °C to ensure that there are no solid TAGs in the oil. All measurements were carried out in triplicates.

Dynamic viscosity. An Anton Paar Rheometer (MCR 302, Anton Paar, Austria) equipped with a cone-plate geometry (50 mm, 1° angle, gap 0.2 mm) and a Peltier system (0–100 °C) was used to determine the dynamic viscosity. The temperature was set to 40 °C, and the measurements were performed at a shear rate of 100 s^{-1} with a constant sample volume of 0.8 ml. Measurements were carried out in triplicates.

Dielectric constant and TPC. A parallel plate type electrode was built with two stainless steel plates. The plates were fixed at a constant distance of 0.5 mm by 4 PTFE washers (Ø 4 mm) and suitable PTFE screws (12 mm in length). Each plate was equipped with a 150 mm stranded wire (cross-sectional area 1.5 mm^2) and connected to a precision LCR meter (4280A, Hewlett Packard). The capacitor was then placed in a sealed PTFE housing filled with the respective oil. The setup and the oil samples were tempered at 20 °C before analysis to ensure a constant and evenly distributed temperature. The variation of the oil temperature during measurements was found to be less than 0.5 °C. The dielectric constant was determined by dividing the capacitance of the oil (C_x) by the capacitance of the air (C_0):

$$\varepsilon = \frac{C_x}{C_0} \quad (1)$$

All measurements were performed at 1 MHz and carried out in triplicates. The content of polar components was determined using a Testo 270 cooking oil tester (accuracy ±1.5 %, Testo SE & Co. KGaA, Titisee-Neustadt).

Fatty acid composition. The fatty acid composition of oils was determined according to DGF method C-VI 10a (00). Briefly, 10-20 mg of oil were dissolved in 3 ml methyl *tert*-butyl ether (HPLC-grade, VWR International Pennsylvania, USA). Consequently, 50 µl of the mix were transferred into 1.5 ml vials with 100 µl inlets, and 30 µl of trimethylsulfonium hydroxide was added. The analysis was performed with a Shimadzu GC 2010 Plus (Shiamdzu, Kyōto, Japan) using a TR-FAME column (length 100 m, Ø 0.25mm, film 0.25µm). All measurements were carried out in triplicates.

2.4 Oleogel analysis

Stock solution preparation. Stock solutions with varying mass fractions of sterol and sterol ester were prepared. Independently of the concentration for each analysis, the molar ratio of sterol and sterol ester was always 1:1 (40:60 mass ratio). The respective amounts were carefully weighed into glass beakers and heated to a maximum of 98 °C after the oil was added on a magnetic stirrer until fully dissolved.

Gel firmness. Freshly prepared 6 % w/w stock solutions were poured into glass Petri dishes (Ø 110 mm) up to a height of 15 mm, cooled to room temperature, and sealed with parafilm. Samples were stored at

5 °C for 7 days before firmness was determined using a static material testing machine (Zwick GmbH & Co. KG, Germany) equipped with a 0.5-inch cylindrical probe. After the preset force of 0.02 N was detected, the cylinder penetrated the sample to a depth of 3 mm, and the force-displacement motions were recorded by the associated program testExpertII. Each sample was penetrated five times, and the distance between each penetration point and the wall of the petri dish was always greater than 10 mm.

Gel-sol transition. Differential scanning calorimetry was performed with a Netzsch 214 Polyma (Netzsch-Gerätebau GmbH, Selb, Germany). 10–15 mg of oleogel (16 % w/w) was cut from the middle of each sample using a scalpel, weighed into aluminum pans, and hermetically sealed. After an isothermal period of 10 min at 20 °C, the samples were heated to 105 °C at a constant rate of 10 °C·min^{-1}. The gel-sol transition temperatures and enthalpies (ΔH_{tot}) were determined using Proteus® software (Netzsch-Gerätebau GmbH, Selb, Germany). Additionally, Gauss curves (ΔH_{peak}) were fitted in the thermograms using PeakFit software (Systat Software GmbH, Erkrath, Germany). The fitted peak represents the dissolution of tubes, which is then used to calculate the peak % of the total dissolution enthalpy [1]:

$$peak\% = \frac{\Delta H_{peak}}{\Delta H_{tot}} \cdot 100 \quad (2)$$

The measurements were carried out in triplicates.

Sol-gel transition and strain sweep. Sol-gel transition temperatures were determined via dynamic mechanical thermal analysis (DMTA) with a plate-plate geometry (gap 0.2 mm). The upper plate was sandblasted to avoid slipping of the sample. Hot oleogel solutions (10 % w/w , 0.8 ml) were pipetted onto the preheated plate (80 °C). Subsequently, the solution was cooled from 80 to 10 °C at a fixed cooling rate of 5 °C/min. The measurements were performed within the LVE at a strain of 0.05 % and an angular frequency of 10 rad/s. The sol-gel transition temperature was calculated using the associated program (Rheoplus, Anton Paar, Austria). It is defined as the crossover of the loss (G") and storage modulus (G') upon cooling. All measurements were carried out in triplicates.
After gelation occurred, the samples were left to rest for 20 min at 20 °C. Then, a strain sweep was performed at 10 rad/s and 20 °C. The data was used to determine G'_{max} and the strain at which the sample starts to be irreversibly deformed (γ_{max}).

Atomic force microscopy (AFM). The network structure was visualized using atomic force microscopy (AFM). Therefore, the method proposed by Matheson, A. B.; Koutsos, V.; Dalkas, G.; Euston, S. and Clegg, P. was used with minor adaptions [16]. A small drop of the hot oleogel solution was applied on freshly cleaved mica sheets (16 % w/w sterols), placed in single-use Petri dishes, and stored at room temperature until gelation occurred. Once the samples were gelled, they were sealed with parafilm and stored at 5 °C for 7 days before analysis. Measurements were performed at the Department of Applied Physical Chemistry at the Technical University Berlin (Prof. Gradzielski) with a Cypher S (Asylum Research, Santa Barbara, CA) atomic force microscope operating in tapping mode. The instrument was equipped with OLYMPUS OMCL cantilevers (model AC160TS-R30, nominal tip radius 7 nm) with a spring constant of 26 N/m and a resonance frequency of 300 kHz. All images were processed and edited using the Gwyddion free software package [17].

3. Results and discussion

3.1 Chemical and physical characterization of oils

Table 1 Chemical and physical parameters of natural (-N), purified (-P) and moisturized (-H2O) canola (C), sunflower (S) and flaxseed (F) oils: TPC- total polar components, ε- dielectric constant, R.I. – refractive index, P.V.- peroxide value, ρ – density, η- dynamic viscosity, H2O- water content, FFA- free fatty acids

sample	TPC %	ε [-]	RI [-]	PV [meq/kg]	ρ [g/cm^3]	η [m·Pas]	H_2O [ppm]	FFA [mg/100g]
C-N	5.0	3.057 ±0.002	1.465 ±7.2·10^{-5}	4.5 ±0.1	0.886 ±5.2·10^{-5}	33.2 ± 0.02	46.8 ±4.4	11.7 ±0.4
C-P	0	3.003 ±0.002	1.456±3.1·10^{-5}	0.5 ±0.1	0.877 ±6.9·10^{-5}	25.5 ±0.02	13.4 ±1.1	n.d.
S-N	7.5	3.183 ±0.001	1.467 ±6.5·10^{-5}	26.6 ±3.4	0.905 ±1.3·10^{-5}	30.4 ±0.05	224.0 ±8.7	75.3 ±2.3
S-P	0	3.010 ±0.003	1.458±4.9·10^{-5}	0.9 ±0.3	0.889 ±5.4·10^{-5}	21.4 ±0.09	19.9 ±1.2	n.d.
F-N	21.5	3.313 ±0.001	1.474 ±2.3·10^{-5}	30.2 ±2.9	0.915 ±4.7·10^{-5}	25.1 ±0.01	326.4 ±11.3	84.4 ±1.8
F-P	8.5	3.200 ±0.004	1.466±8.2·10^{-5}	22.6 ±1.4	0.908 ±6.9·10^{-5}	17.7 ±0.07	17.1 ±4.2	n.d.

Table 1 shows oil quality parameters before and after the purification. The treatment significantly reduced chemical compounds such as free fatty acids, water, and peroxides. Tocopherols were not determined in this study, but it has been shown that they are drastically reduced or eliminated by purification [1]. Moreover, the elimination of polar components results in a decline of some physical parameters such as viscosity, permittivity (and % TPC), density, and refractive index. It needs to be mentioned that purified flaxseed oil does not contain 8.5 % TPC. The FAs of flaxseed oil have significantly more double bonds (see IVs below) mainly due to the high content of linolenic acid (~50 %). More double bonds result in a higher permittivity [18]. The Testo cooking oil tester correlates the permittivity measured to a reference oil, which features a lower permittivity since it consists of 87 % oleic acid. Consequently, the output for purified flaxseed oil must be > 0 %. That underlines the Testo's limitations for determining polar compounds in oils having different FA compositions than the reference oil.

The treatment considerably reduced or eliminated minor components such as free fatty acids, water, and peroxides. The solvent's polarity expressed as dielectric constant decreased since molecular species with a greater polarity than TAGs were removed (e.g., water, fatty acids). Consequently, the permeability of the liquid permittivity of the liquid decreases when an electric field is applied. That is also reflected in the decline of the refractive index: when mobile charge carriers are present, the electromagnetic field's diffusion is compensated, and the phase velocity of light through the medium declines ($n = c_0/c_m$). Hence, the refractive index is lower after oil purification.

It is stated that purification with activated alumina and silica gel does not alter plant oils' fatty acid composition [15, 19]. Indeed, Table 2 verifies that fatty acid compositions did not change considerably by the treatment. The data obtained by gas chromatography was used to calculate iodine values of purified canola (134), sunflower (158), and flaxseed oil (223).

Besides, it was found that oils purified in the same manner contained no copper or iron as well as sterols [19, 20]. Interestingly, purified flaxseed oil still contained considerable amounts of peroxides after purification (22.6 meq/kg). That is likely related to the strong oxidative potential of linolenic acid. Thus, peroxides could have formed during solvent distillation at 45 °C, although exposure to oxygen and elevated temperatures were kept as short as possible. A higher level of degradation products such as peroxides results in an increase in oil density due to the formation of conjugated monoenes, dienes, and trienes. These exhibit a lower molar volume and, thus, higher density [21].

Table 2 Fatty acid profile [%] of natural (-N), purified (-P) canola (C), sunflower (S) and flaxseed (F) oils

sample	16:0	18:0	18:1	18:2	18:3	20:1
C-N	4.8 ± 0.08	2.2 ± 0.06	62.1 ± 0.12	24.1 ± 0.07	5.4 ± 0.17	1.3 ± 0.03
C-P	4.6 ± 0.03	2.3 ± 0.05	62.1 ± 0.05	24.3 ± 0.05	5.3 ± 0.02	1.4 ± 0.04
S-N	5.8 ± 0.04	3.2 ± 0.02	32.5 ± 0.07	58.6 ± 0.06	n.d.	n.d.
S-P	5.7 ± 0.01	3.1 ± 0.00	33.1 ± 0.06	58.2 ± 0.06	n.d.	n.d.
F-N	5.7 ± 0.01	4.3 ± 0.01	20.5 ± 0.07	14.6 ± 0.05	49.9 ± 0.07	4.9 ± 0.05
F-P	5.6 ± 0.03	4.4 ± 0.01	22.0 ± 0.11	14.7 ± 0.11	48.3 ± 0.23	4.8 ± 0.25

3.2 Oleogels from purified oils

Figure 1 depicts the gel-sol and sol-gel transition temperatures (top left and right), the dissolution enthalpy (bottom left), and oil viscosity and oleogel firmness (bottom right). The data in this section is always plotted against the iodine value of the respective purified oil. As mentioned in the previous section, the oil density and permittivity increase with double bonds while oil viscosity decreases (Table 1). In line with that, sol-gel transition temperatures increased slightly with iodine value since a lower viscosity enables a higher diffusion rate. Thus, the probability of encountering during the self-assembly of the sterol and sterol ester molecules increases. Interestingly, the gel-sol transition temperature decreases from 80.5 °C (canola) to 77.1 °C (flaxseed). That implies a decrease in the amount of tubules with iodine value since the peak dissolution temperature can be associated with the tubules' disappearance and hence their concentration in the gel [1, 22].

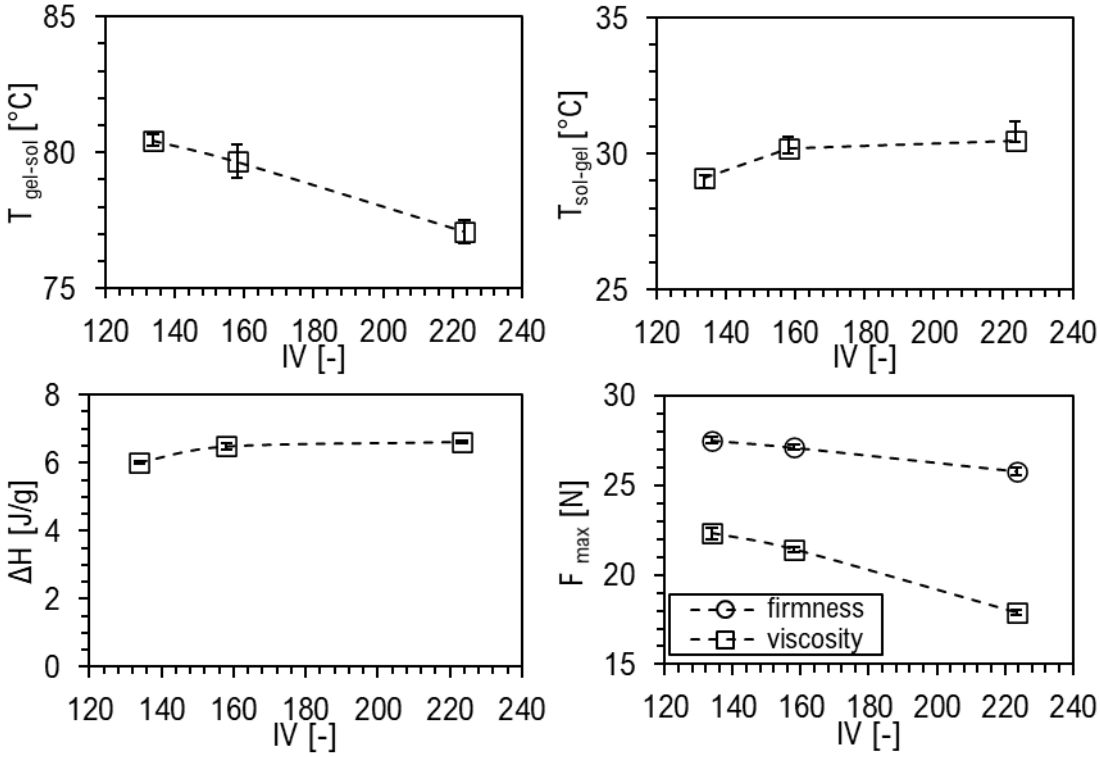

Figure 1 Gel-sol (top left) and sol-gel transition temperature (top right), dissolution enthalpy (bottom left) of oleogels and oil viscosity and oleogel firmness (bottom right) of purified canola, sunflower and flaxseed oil, lines to guide the eye

In contrast, the dissolution enthalpy somewhat increases with iodine value, indicating that more energy is needed for the gel-sol transition (Figure 1, bottom left). That suggests more or stronger interactions within the network, which does not seem logical at first glance. Distinct effects could cause this: The decline in solvent viscosity enables more flexibility of the tubules and bundles, resulting in more interaction points. Secondly, the solvent's polarity, expressed as permittivity, increases with the iodine value (Table 1). This could result to variation of the solubility of the structurants in the continuous phase resulting in a change in the number of scaffolding elements. However, assuming that more tubules in flaxseed and sunflower oil than in canola oil is in conflict with the observation of reducing gel-sold transition temperatures. That is in line with oryzanol's solubility increase with increasing solvent polarity, resulting in fewer tubules as described in the introduction.

Lastly, primary oxidation products (peroxides) were present in purified flaxseed oil. Additionally, the oleogel preparation procedure at elevated temperatures could promote their formation, especially in flaxseed and sunflower oil. These might promote interactions between adjacent tubules and bundles, considerably changing the network's appearance (bundle thickness, branching) and its macroscopic properties [1].

That is in line with results obtained by dynamic molecular modeling reported recently by Matheson et al. [9]. They partially exchanged triglycerides with glycerol (ε~46.5), which led to a disruption of inter-tubule

interactions in favor of glycerol interacting with the hydroxyl group of sitosterol and the methoxy, phenol and carbonyl groups of oryzanol. Although these boosted the individual tube's stability (intra-tube), the system's network strength is predominately generated via (inter-tube) interactions. Besides, the reinforcement is counterbalanced by the lack of tubes in glycerol, indicated by a sharp decline in storage modulus above 28 % w/w glycerol substitution [9]. Unfortunately, glycerol was only added to the triglyceride oil in large amounts (15-50 % w/w). Hence, it remains unclear whether there is a dose-dependent effect at low substitution levels. In that case, a network strengthening effect appears likely due to the formation of moderate numbers of hydrogen bonds on the tube surface, increasing their stability and leaving sufficient binding points for inter-tube connections.

In line with that, oleogel firmness decreased with increasing iodine value (Figure 1 Gel-sol (top left) and sol-gel transition temperature (top right), dissolution enthalpy (bottom left) of oleogels and oil viscosity and oleogel firmness (bottom right) of purified canola, sunflower and flaxseed oil, lines to guide the eyeFigure 1, bottom right). Therefore, it seems that gel hardness in purified oils seems to be related to potential changes in network appearance due to modified interactions of scaffolding elements. Moreover, the decrease of oil viscosity with IV could add to the observation (Figure 1, bottom right). In contrast, it has been reported for EC oleogels that firmness increased with the number of double bonds [21]. The authors claimed that the polymer-solvent interactions are a function of the molar volume of the solvent. Consequently, EC strands are more separated in oils with fewer double bonds, which results in larger network pores and softer gels. Unfortunately, the oils in this study were not standardized. Hence, different effects caused by minor oil components and solvent composition might coincide and cause the increase of oleogel firmness. Nevertheless, this underlines the importance of understanding the relation of oil composition, network structure, and interactions within the oleogel.

Bot, A., den Adel, R. and Roijers, EC reported that the gel-sol transition process starts at temperatures far lower than the peak dissolution temperature [23]. In a later study, this peak fronting was linked to the breakup of inter-tubule interactions (weaking of the network), while the peak temperature relates to the dissolution of tubules (intra-tube interactions) [1]. The latter includes the disintegration of the intramolecular hydrogen bond responsible for stacking of the sterol and the sterol ester and weak interactions formed between ferulic acid moieties within one tubulel [1, 8, 23]. Consequently, the peak area likely connects to the dissolution of tubes while the remaining energy is needed to break down inter-tube bonds formed between adjacent tubes. The authors further reported an increase of the fronting with increasing levels of minor components in the oil and a simultaneous decrease of the peak area resulting in a reasonably constant total dissolution enthalpy for all samples [1].

Thus, the DSC thermograms of purified oils were analyzed using PeakFit software. A modifiable Gaussian curve was fitted into each thermogram. Figure 2 exemplifies a fit of an oleogel from purified canola oil. Consequently, the peak area % was calculated according to Equation 2. The data can be used to disentangle the effect of TAG composition from the contribution of minor components, which potentially form during oleogel preparation. An increase in fronting area and decrease in peak area might explain the decrease in gel-sol transition temperature and concurrent increase of dissolution enthalpy with IV.

Table 3 holds the average percentage of the peak area for all three oils. The peak area % and the total peak area are negatively correlated to the IV, although the total dissolution enthalpy increased slightly (Table 3, Figure 1). Hence, the decline in gel-sol transition temperature and peak enthalpy indicates that the concentration of tubules in the gel decreases with iodine value.

It is conceivable that this is the result of a modified solubility of one or both structurants. To this end, β-sitosterol was added to purified oils (x_{sito}=0.3; ~20 % w/w) and subjected to a heating-cooling-heating program. Unfortunately, oryzanol did not exhibit a clear signal in DSC upon cooling, which is likely

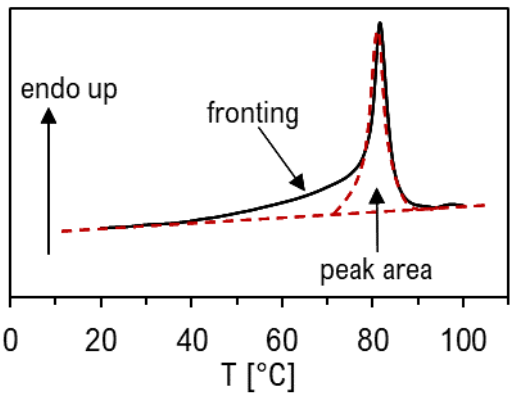

Figure 2 Exemplary fit (Peakfit software) of peak area and fronting in purified canola oil, similar thermograms were obtained for purified sunflower and flaxseed oil

related to the diversity of the molecular species and their complex crystallization behavior, resulting in an extended period needed for the phase transition. Indeed, it has been reported that crystallization of oryzanol fractions from rice bran oil soapstocks is a very time-consuming method [24, 25]. Consequently, the procedure to determine phase transition temperatures had to be modified. The oil and phytosterol esters (x_{ory}=0.3; ~29 % w/w) were first heated to 70°C until dissolved and subsequently stored at ambient temperature for 7 days before DSC measurements.

Solidification temperatures of sitosterol increase with IV, similarly to those reported for oleogels (Figure 1), which is likely related to the solvents' viscosity (Table 3). Table 3 further shows that melting temperatures of sitosterol and oryzanol crystals increases with iodine value. This indicates the structurants' solubility decrease with iodine value in line with oryzanol solubility results mentioned earlier [11]. That is also reflected in the increase in transition enthalpy (only sitosterol). The transition enthalpy of oryzanol appears invariable with iodine value. Still, the data showed a larger deviation since the values are at the lower end of the differential scanning calorimeter's confidence range. The data indicate that with decreasing IV, more structurants remain dissolved in the oil. Hence, slightly fewer tubes are available to gel the oil. That is contrary to the decrease in gel-sol transition temperature (Figure 1, top left). Potentially, the lower network strength and higher oil viscosity enable a quicker dissolution of inter-and intra-tube interactions. That might cause the decrease in peak area and simultaneous growth of the peak fronting reported earlier (Table 3). A similar effect has been reported for oils with high levels of deterioration products [1]. Here, a shift from intra- to inter-tubule interactions was assumed, expressed in the same shift from peak to fronting area while the transition enthalpy was reasonably constant. After all, the gels' disintegration upon heating can be considered the dissolution of tubes in the continuous phase, which is likely related to their molecular mobility.

Moreover, it is arguable whether the transition temperatures of pure components relate to the mixture's self-assembling process. Although both processes are enthalpy driven, the mixture must be less soluble so that the formation of tubules is energetically favorable [10]. Indeed, the gel-sol ?? transition temperatures of mole fractions equal to a 16 % w/w gel (x=0.11 equimolarly) computed assuming ideal solubility are 24.5, 19.2, and approximately 30 °C for sitosterol, and oryzanol, and oleogel, respectively. In summary, the effects observed for the pure components do not explain the decrease in gel-sol transition temperatures of the mixture sufficiently. Nevertheless, changes appear insignificant compared to modifications by polar components, as we showed in the second part of this study.

Table 3 Phase transition enthalpies and temperatures of 16 % w/w oleogels, x=0.3 β-sitosterol or γ-oryzanol in purified oils, ΔH_{peak}, $\Delta H_{fronting}$ were determined using PeakFit software, T_m – melting temperature, T_c -crystallization temperature, ΔH_m -melting enthalpy

		C-P	S-P	L-P
oleogel 16 % w/w	ΔH_{total} [J/g]	6.01 ±0.1	6.49 ±0.2	6.62 ±0.3
	ΔH_{peak} [J/g]	3.16 ±0.003	2.91 ±0.200	2.61 ±0.037
	$\Delta H_{fronting}$ [J/g]	2.85 ±0.01	3.58 ±0.07	4.02 ±0.21
	peak [%]	53.3 ±1.4	52.7 ±1.7	46.7 ±2.4
	fronting [%]	46.7 ±1.4	47.3 ±1.7	53.3 ±2.4
β-sitosterol 20 % w/w ; x=0.3	T_m [°C]	91.03 ±1.7	95.55 ±0.05	96.90 ±1.3
	T_c [°C]	78.73 ±1.0	81.25 ±1.8	86.35 ±1.3
	ΔH_m [J/g]	8.01 ±0.5	8.28 ±0.5	9.15 ±0.2
γ-oryzanol 29 % w/w; x=0.3	T_m [°C]	59.75 ±0.9	62.55 ±1.3	64.23 ±0.7
	ΔH_m [J/g]	2.30 ±0.53	2.00 ±0.40	2.19 ±0.21

Besides penetration and back extrusion tests, the gels' deformation characteristics can be assessed using large deformation rheology such as amplitude sweeps. Moreover, the results provide more detailed information about network properties, allowing for evaluating the connection points of the structural elements and their breakdown characteristics. The deflection can be operated at two pre-settings: controlled shear deformation (CSD) and controlled shear stress (CSS). The typical stress response of a gel shows a plateau region of the storage and loss modulus (G' and G") at low stress (Figure 3). As the stress increases, the gel is no longer able to store the deformation energy, which is accompanied by a

decline in G' and sometimes a maximum of G "(due to friction of loose structures). As the strain increases further, the viscous behavior begins to dominate, and the sample starts to flow at G'=G" (flow point). The storage modulus within the linear viscoelastic region (LVE) can be associated with the gel's stiffness and the number of junction points in the network. The curve declines continuously once brittle fracturing occurs in the sample (for gels, usually $\gamma_{max} \approx 0.5$ %), indicating a gradual breakdown of the structure.

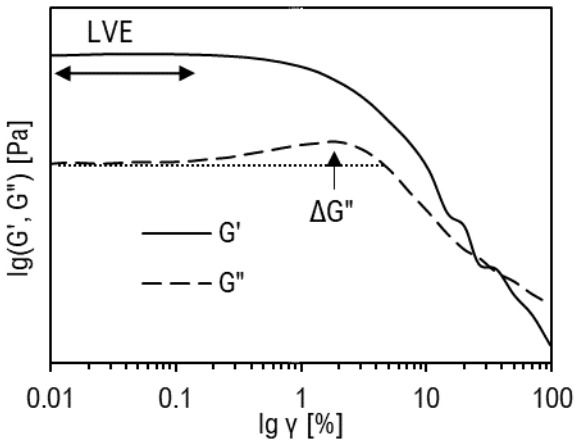

Figure 3 Exemplary plot of a sterol/sterol ester oleogel during strain sweep

In contrast, the loss modulus (G") increases above γ_{max} until reaching a distinct maximum and then declines less sharply than G'. The extent of the maximum (ΔG") is related to the amount of deformation energy (internal friction) that is lost due to the break up of individual bonds and the formation of independent aggregates in micro-cracks of the network. These fragments are no longer incorporated in the network structure, although the surrounding material is still firm[26]. Consequently, a larger ΔG" might relate to a network structure forming weaker bonds, resulting in a more significant fragments formation.

However, a gel that exhibits G'>G" in the LVE and shows a distinct maximum of G" exhibits a steady, three-dimensional network under quiescent conditions. The breakup of the structure takes place with some delay due to the fragment formation. Macro cracks finally cause the rupture of the entire network, and the viscous behavior prevails. A gel's behavior under increasing strain is crucial for successful product development since most food production processes involve shearing. Moreover, natural minor oil components and deterioration products significantly modify the gels' stress response and macroscopic network properties [27].

Figure 4 depicts the changes in maximum storage modulus G'_{max} and stress limit (γ_{max}) of the LVE for oleogels from purified canola, sunflower, and flaxseed oil. The maximum storage modulus (G'_{max}) in the linear viscoelastic region is practically identical for all three oils. Bearing in mind that there are fewer tubules in oleogels from flaxseed oil, it can be hypothesized that there is more cross-linking between adjacent tubules and bundles. That is in line with the effects reported for the dissolution enthalpy and indicates a greater number of junction zones in the network. These can result from a higher content of primary oxidation products and lower oil viscosity. In compliance, the maximum strain in the LVE seems to decrease slightly with the IV. Consequently, the network junction zones (microscopic level) break down more readily when subjected to stress. On a macroscopic level, this appears to correspond with a lower gel firmness (Figure 1).

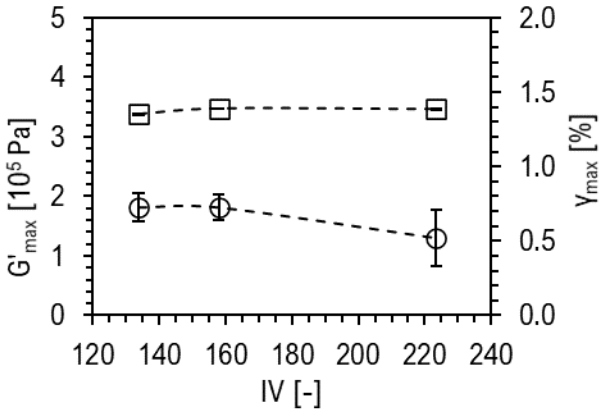

Figure 4 Maximum storage modulus (squares, G'_{max}) and maximum strain (circles, γ_{max}) in the linear viscoelastic region (LVE) of 10 % w/w oleogels from purified canola, sunflower and flaxseed oil, lines to guide the eye

At this point, it remains unclear if the changes in gel dissolution and network properties solely arise from the properties of the bulk solvent - mainly polarity and viscosity – which are determined by the triglyceride composition. Another possibility is the interactions of primary oxidation products with the ferulic acid moiety of oryzanol. These are formed rapidly in oils rich in polyunsaturated acids when subjected to high temperatures. The differences might be visible in the network structure and arrangement of tube-bundles. To this end, atomic force microscopy was performed.

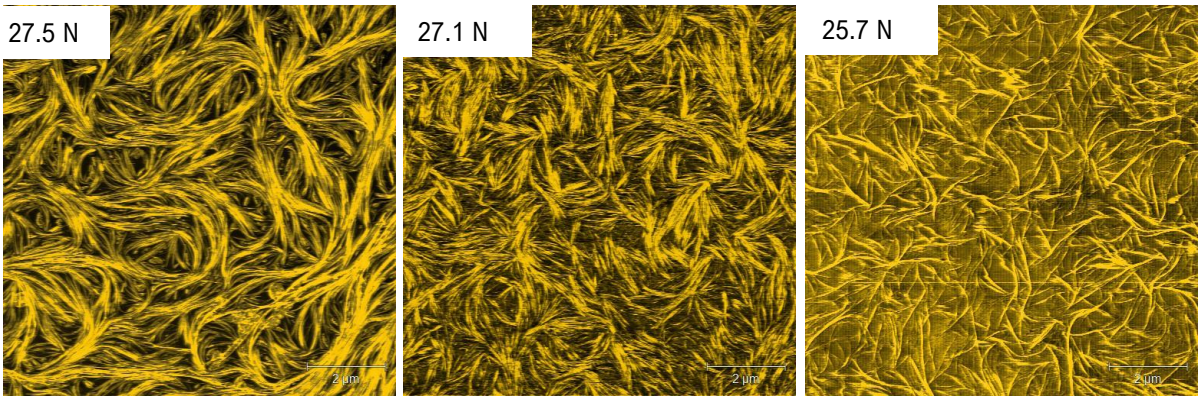

Figure 5 AFM-micrographs of oleogels with 16 % w/w β-sitosterol/γ-oryzanol (1:1 molar ratio) from purified canola (left), sunflower (middle) and flaxseed oil (right), hardness value displayed in top left corner, scanning size 10µm

3.3 Microstructure of oleogels

Atomic force microscopy (AFM) was used to obtain information about the network arrangement on the surface of oleogels. Several studies showed that AFM is a powerful tool to visualize these structures with a lower risk of artifacts due to sample preparation than scanning electron microscopy [1, 16, 28]. Additionally, the micrographs allow for the size and height determination of sterol/sterol ester tubes and their bundles. High-resolution images confirmed previously generated SAXS data from which a single tubule's size was determined [1, 16, 23]. On the downside, AFM only depicts a sample's surface, and thus no information about the spatial arrangement of the structural elements can be obtained. For the same reason, the length of tube bundles cannot be determined.

Figure 5 shows AFM micrographs (10 µm scanning size) of oleogels with 16 % w/w structurants made with purified oils with different degrees of unsaturation (increasing iodine value from left to right). For comparison, Figure 6 shows a 16 % w/w oleogel from untreated canola oil. Fibrous textures can be seen in all pictures, although they seem to pack and branch considerably differently. In the sample containing untreated canola oil (Figure 6), the surface is packed with bundles that are twisted and align and exhibit numerous intersections. Similar results have been described in other studies [1, 8, 9]. Micrographs of oleogels from untreated sunflower and flaxseed oil showed very similar arrangements (data not shown). Reportedly, minor polar components might accumulate on the tubule surface due to weak interactions with oryzanol's ferulic acid moiety [1, 9]. Consequently, dense bundles with numerous junction zones and areas of alignment were observed. In contrast, it was reported that bundles in gels in which purified oils were utilized appeared more randomly distributed, and fewer bundles were visible, which was indicated by larger dark areas [1].

However, in that study, only one micrograph per sample was taken. Moreover, insufficient sample preparation only allowed for visualization at the sample's very edges since smooth areas could not be found elsewhere. The issues mentioned above were addressed, and sample preparation was optimized for the study presented here. Consequently, the micrographs in 5 appear significantly different. For this study, at least 6 images were taken from each sample. Moreover, oleogels with 16 % w/w sterol/sterol ester were used for AFM, making it more challenging to determine bundle arrangement changes due to the dense tubule packing at the surface. However, AFM measurements could not be performed with samples containing 6 % w/w sterol mixture (used for firmness measurements) because there was no interaction between tip and sample. Nevertheless, gel firmness and transition temperatures decreased similarly in oleogels with 16 % w/w sterols (data not shown). Consequently, comparable changes in the arrangement of the scaffolding elements can be assumed.

The surface of purified canola oil oleogels oil exhibits large areas of tubule alignment into thick bundles (size range 48-1170 nm) and branching. A similar arrangement is visible in purified sunflower oil oleogels (Figure 5, middle), although bundles appear shorter and less twisted (size range 47-1127 nm). In contrast, to canola and sunflower, oleogels from purified flaxseed oil appear to have fewer and thinner bundles on the surface (Figure 5, right). However, that impression might be misleading since it could result from oil migrating to the gel surface due to the lower gel firmness, insufficient oil binding capacity,

and lower viscosity of the continuous oil phase. Indeed, it was more difficult to obtain useful micrographs from flaxseed oil oleogels because of lower tip-sample interactions.
Nevertheless, the differences in spatial arrangement might also arise from the formation of primary oxidation products. It was mentioned in section 3.1that these form rapidly in oils with a high content of polyunsaturated fatty acids. Consequently, peroxides likely develop during oleogel preparation (98 °C) in purified sunflower and flaxseed oil. These polar compounds do not alter the molecular stacking of sitosterol and oryzanol, and hence the general tube structure is maintained. However, due to their polar nature, they likely interact with oryzanol's ferulic acid moiety, which protrudes into the continuous liquid phase. Because the acid moiety can form weak connections with surrounding molecules, it is considered the critical element for inter-tube interactions [8, 9]. Consequently, the polar components could modify inter-tube interactions and bundle arrangement.

4. Conclusion

The iodine value of purified triglyceride oils has a limited impact on γ-oryzanol/β-sitosterol oleogel structure and properties, contrasting with the effects reported for ethylcellulose oleogels [20]. The results collected in this study showed that the bulk's viscosity is more relevant for network formation and firmness than the triglyceride composition. However, a decrease in firmness and the gel-sol transition was observable. That is likely linked to the rapid formation of primary oxidation products in oils with a high polyunsaturated fatty acid content. Hence, the transition enthalpy and maximum storage modulus in the LVE increased with iodine value associated with an increase in tube-tube interactions in the presence of peroxides.

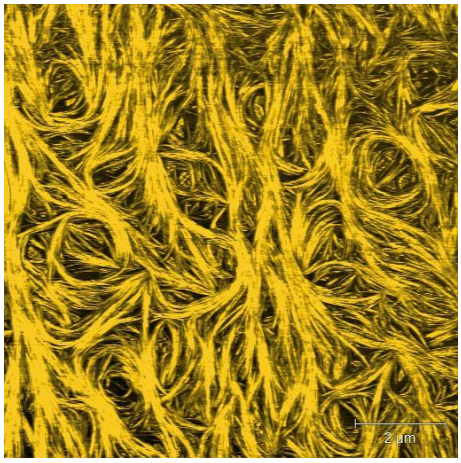

Figure 6 AFM micrograph of a 16 % w/w oleogel (sitosterol/oryzanol, 1:1 molar ratio) made with untreated canola oil

The decrease of the peak area in DSC thermograms and a simultaneous increase in the peak fronting further supported this hypothesis since the peak fronting was associated with the breakdown of weak inter-tube interactions. In contrast, the peak area represents the dissolution of the tubes, mainly the breakup of the hydrogen bond between oryzanol and sitosterol. The lower gel-sol transition temperature and total peak area in oils with a high iodine value and peroxides indicate fewer tubes in the gel.
Indeed, AFM-micrographs indicate a less packed surface in flaxseed oil oleogels and a drastic decrease in bundle size. That could also result from oil migrating to the gels' surface due to a weaker network in oleogels from flaxseed oil. The interactions of the AFM-tip with the sample were weak supports this hypothesis. Nevertheless, the general arrangement is likely linked to the rapid formation of hydroperoxides in flaxseed oil. Consequently, this gel's surface was more similar to the curled structure observed in natural canola oil (Figure 5 and Figure 6) than gels from the other purified oils. In oleogels from purified canola and sunflower oil tubes seem to be glued together in very thick strands.
Interestingly, the maximum storage modulus showed a slight increase with iodine value, while the γ_{max} % of the linear viscoelastic region decreased. Hence, the number of network junction points increased. Still, the structure breaks up more readily when subjected to increasing oscillation stress, which might be linked to structures loosely incorporated into the network.
From previously published results and this study, it can be concluded that the impact of triglyceride composition (expressed as iodine value) is inferior to the effect of minor oil components [1].
It will remain challenging to disentangle all factors affecting oleogels connected to the continuous phase composition and link the results comprehensively since effects appear simultaneously. However, understanding the basic principles of, for example, sol-gel transition and how they can be manipulated is inevitable to implement oleogels in production processes successfully. Hence, the second part of this study aims to understand the effects of selected minor components on sterol/sterol ester networks. To

this end, molecular species related to edible oils but with different functional groups were added to purified oils at varying concentrations. Consequently, oleogels were prepared and analyzed similarly to this study.

References

1. Scharfe M, Ahmane Y, Seilert J et al. (2019) On the effect of minor oil components on β -sitosterol/γ -oryzanol oleogels. Eur J Lipid Sci Technol. https://doi.org/10.1002/ejlt.201800487
2. Fry AC, Bonner E, Lewis DL et al. (1997) The effects of gamma-oryzanol supplementation during resistance exercise training. Int J Sport Nutr 7:318–329
3. Gerhardt AL, Gallo NB (1998) Full-fat rice bran and oat bran similarly reduce hypercholesterolemia in humans. J Nutr 128:865–869. https://doi.org/10.1093/jn/128.5.865
4. Yoshino G, Kazumi T, Amano. M et al. (1989) Effects of gamma-oryzanol on hyperlipidemic subjects. Current Therapeutic Research, Clinical & Experimental 45:543–552
5. Eslami S, Esa NM, Marandi SM et al. (2014) Effects of gamma oryzanol supplementation on anthropometric measurements & muscular strength in healthy males following chronic resistance training. Indian J Med Res 139:857–863
6. Katan MB, Grundy SM, Jones P et al. (2003) Efficacy and safety of plant stanols and sterols in the management of blood cholesterol levels. Mayo Clinic Proceedings 78:965–978. https://doi.org/10.4065/78.8.965
7. Bot A, Gilbert EP, Bouwman WG et al. (2012) Elucidation of density profile of self-assembled sitosterol + oryzanol tubules with small-angle neutron scattering. Faraday Discuss 158:223. https://doi.org/10.1039/c2fd20020a
8. Dalkas G, Matheson AB, Vass H et al. (2018) Molecular Interactions behind the Self-Assembly and Microstructure of Mixed Sterol Organogels. Langmuir 34:8629–8638. https://doi.org/10.1021/acs.langmuir.8b01208
9. Matheson A, Dalkas G, Mears R et al. (2018) Stable emulsions of droplets in a solid edible organogel matrix. Soft Matter 14:2044–2051. https://doi.org/10.1039/c8sm00169c
10. Sawalha H, Margry G, den Adel R et al. (2013) The influence of the type of oil phase on the self-assembly process of γ-oryzanol + β-sitosterol tubules in organogel systems. Eur J Lipid Sci Technol 115:295–300. https://doi.org/10.1002/ejlt.201100395
11. Cuevas MA, Shinzat RE, Costa MC et al. (2011) Gamma-oryzanol Solubility and Effect of Solvents Mixture. International Congress of Food and Engineering:1–3
12. Calligaris S, Mirolo G, Da Pieve S et al. (2014) Effect of Oil Type on Formation, Structure and Thermal Properties of γ-oryzanol and β-sitosterol-Based Organogels. Food Biophysics 9:69–75. https://doi.org/10.1007/s11483-013-9318-z
13. Bot A, Agterof WGM (2006) Structuring of edible oils by mixtures of γ-oryzanol with β-sitosterol or related phytosterols. J Am Oil Chem Soc 83:513–521. https://doi.org/10.1007/s11746-006-1234-7
14. Lampi A-M, Kamal-Eldin A (1998) Effect of α- and γ-tocopherols on thermal polymerization of purified high-oleic sunflower triacylglycerols. J Amer Oil Chem Soc 75:1699–1703. https://doi.org/10.1007/s11746-998-0319-x
15. Mariod A, Matthäus B, Hussein IH (2011) Effect of Stripping Methods on the Oxidative Stability of Three Unconventional Oils. J Am Oil Chem Soc 88:603–609. https://doi.org/10.1007/s11746-010-1703-x
16. Matheson AB, Koutsos V, Dalkas G et al. (2017) The microstructure of β-sitosterol: γ-oryzanol edible organogels. Langmuir 33
17. Nečas D, Klapetek P (2012) Gwyddion: An open-source software for SPM data analysis. Open Physics 10:99. https://doi.org/10.2478/s11534-011-0096-2

18. Lizhi H, Toyoda K, Ihara I (2008) Dielectric properties of edible oils and fatty acids as a function of frequency, temperature, moisture and composition. Journal of Food Engineering 88:151–158. https://doi.org/10.1016/j.jfoodeng.2007.12.035
19. Warner K (2005) Effects on the flavor and oxidative stability of stripped soybean and sunflower oils with added pure tocopherols. J Agric Food Chem 53:9906–9910. https://doi.org/10.1021/jf0517593
20. Baldioli M, Servili M, Perretti G et al. (1996) Antioxidant activity of tocopherols and phenolic compounds of virgin olive oil. J Am Oil Chem Soc 73:1589–1593. https://doi.org/10.1007/BF02523530
21. Laredo T, Barbut S, Marangoni AG (2011) Molecular interactions of polymer oleogelation. Soft Matter 7:2734. https://doi.org/10.1039/c0sm00885k
22. Sawalha H, Venema P, Bot A et al. (2011) The Influence of Concentration and Temperature on the Formation of γ-Oryzanol + β-Sitosterol Tubules in Edible Oil Organogels. Food Biophysics 6:20–25. https://doi.org/10.1007/s11483-010-9169-9
23. Bot A, den Adel R, Roijers EC (2008) Fibrils of γ-Oryzanol + β-Sitosterol in Edible Oil Organogels. J Am Oil Chem Soc 85:1127–1134. https://doi.org/10.1007/s11746-008-1298-7
24. Narayan AV, Barhate RS, Raghavarao KSMS (2006) Extraction and purification of oryzanol from rice bran oil and rice bran oil soapstock. J Am Oil Chem Soc 83:663–670. https://doi.org/10.1007/s11746-006-5021-2
25. Narayan AV, Barhate RS, Inidra TN et al. (2002) Process for crystallization of oryzanol from oryzanol enriched fraction derived from rice bran oil soap stock(WO2004/055040A1). https://patentimages.storage.googleapis.com/2f/ce/7c/47137f76d0a500/WO2004055040A1.pdf
26. Mezger TG (2016) Das Rheologie Handbuch: Für Anwender von Rotations- und Oszillations-Rheometern. FARBE UND LACK // BIBLIOTHEK. Vincentz Network, Hannover
27. Scharfe M (2019) On the importance of minor components and oil properties for oleogel strength, Sevilla
28. Giacintucci V, Di Mattia CD, Sacchetti G et al. (2018) Ethylcellulose oleogels with extra virgin olive oil: the role of oil minor components on microstructure and mechanical strength. Food Hydrocolloids 84:508–514. https://doi.org/10.1016/j.foodhyd.2018.05.030